Fermi National Accelerator Laboratory

FERMILAB-Conf-95/037

Backgrounds and Detector Performance at a 2 x 2 TeV $\mu^+\mu^-$ Collider

G. William Foster and Nikolai V. Mokhov

Fermi National Accelerator Laboratory
P.O. Box 500, Batavia, Illinois 60510

March 1995

To be published in *Proceedings of the 2nd Workshop on Physics Potential & Development of mu+ mu- Colliders*, Sausalito, California, November 17-19, 1994

Backgrounds and Detector Performance at a 2×2 TeV $\mu^+\mu^-$ Collider

G. William Foster and Nikolai V. Mokhov

Fermi National Accelerator Laboratory

P.O. Box 500, Batavia, Illinois 60510

INTRODUCTION

The rich physics potential of a high-energy high-luminosity $\mu^+\mu^-$ collider and the surprising feasibility of a design [1, 2] attract the attention of many people these days. A few issues define the practicality of such a project, with the enormous particle background levels in a detector due to unavoidable reasons holding first place. In contrast to hadron colliders where particle backgrounds come both from interaction point (IP) and accelerator [3], almost all the backgrounds in the muon collider detectors arise in the machine. The decay length for 2 TeV muons is $\lambda_D^{-1} \sim 10^{-7}m^{-1}$. With 10^{12} muons in a bunch one has 10^5 decays per meter in a single pass through an interaction region, and 10^8 decays per meter per 12 msec store.

This paper examines two major classes of detector backgrounds presented in the muon collider: beam halo backgrounds, and the "direct" backgrounds from electrons from $\mu \rightarrow e\nu\tilde{\nu}$ decay occurring in the beam channel. We describe the nature of both of these backgrounds, provide results of first realistic calculations for both sources and discuss their effects on plausible detectors. Various shielding and collimation geometries have been simulated, and their efficacy and the nature of the surviving background discussed.

DESCRIPTION OF SIMULATIONS

In this paper we study beam muon decays and beam halo interactions in the inner triplet region $\pm 70m$ from the IP. The lattice calculated by B. Palmer and used in our calculations, provides $\beta^* = 3mm$ with $\beta_{peak} = 400km$ at $Q1-B2$ location (Fig. 1). Superconducting dipole magnets B1, B2 and B3 have central field 8 T. Combined function superconducting quadrupoles Q1 and Q2 are with 2 T dipole component and a gradient of 50 T/m. All of the SC components have 8 cm radius aperture.

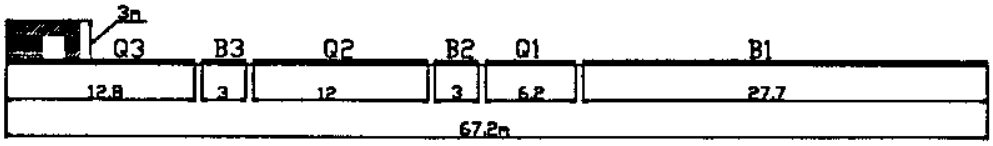

FIGURE 1. Muon collider inner triplet. Dimensions are in meters.

The Q3 quadrupole is resistive with 0.5 T dipole field, except the first 1.3 m near the IP where the dipole component is equal to zero. Its aperture is reduced toward the IP from R=4.5 cm at L=12.8 m to R=0.45 cm at L=1.2 m (see Fig. 2), with the gradient growing from 33.3 T/m to 333.3 T/m, appropriately. Geometries and materials of beam pipes, collars, yokes and cryostats for SC bending dipoles and combined function quadrupoles as well as 2-D POISSON calculated magnetic fields in these components are embedded in the calculational package.

A rather simple model detector is used in this study (Fig. 2): a two-region silicon tracker with volume averaged density $\rho = 0.15 g/cm^3$, a central calorimeter (CH, $\rho = 1.03 g/cm^3$) and a solenoid magnet with 2 Tesla magnetic field. A copper bucking coil is placed on the outside of the Q3 to neutralize the effect of the solenoidal field in the quadrupole.

All the calculations are done with MARS95 code [4], the newest version of the MARS system [5]. Improvements relevant to this problem include better description of muon cross-sections, of muon decay and of the algorithm for electromagnetic fluctuations [6]; improved particle transport algorithm in a magnetic field; synchrotron radiation generation; modified geometry description; extended histogramming and graphical possibilities. The calculation for each case consists of:

- forced $\mu \rightarrow e\nu\tilde{\nu}$ decays in the interaction region (IR) beam pipe;
- tracking of created electrons in the beam pipe under influence of the magnetic field with emission of the synchrotron photons along the track;
- simulation of electromagnetic showers in the triplet and detector components induced by electrons and synchrotron photons hitting the beam pipe;
- simulation of muon interactions (bremsstrahlung, direct e^+e^- pair production, ionization, deep inelastic nuclear interactions and decays) along the tracks in the lattice and detector;
- simulation of electromagnetic showers in the triplet and detector components created at the above muon interaction vertices;
- histogramming and analysis of particle energy spectra, fluences and energy deposition in various detector regions as well as in the whole IR.

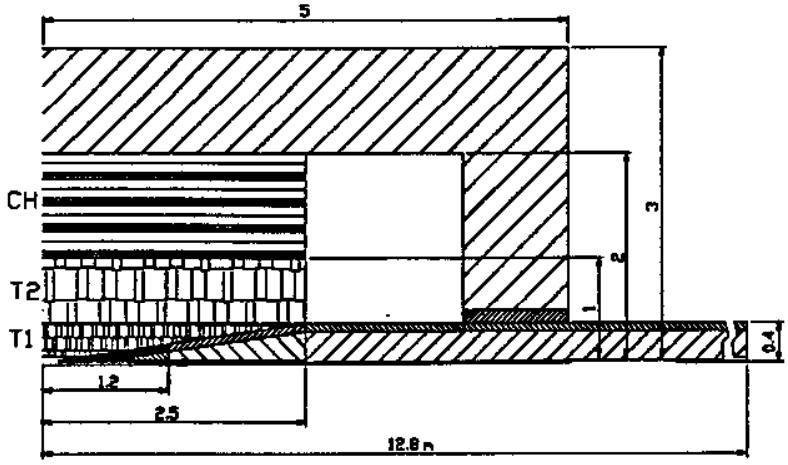

FIGURE 2. Detector, Q3 quadrupole and nozzle configuration used in this study. Dimensions are in meters.

Estimation is done for photo-muon and photo-hadron production including giant resonant neutrons. Energy thresholds are 1 MeV for muons and charged hadrons, 0.1 MeV for electrons and photons, and 0.5 eV for neutrons. In this paper we present results only for electromagnetic component ($e^{\pm}, \gamma$) with $E > 0.5\ MeV$.

In this study we assume that a bunch of $10^{12}, 2\ TeV$ muons pass from right to left toward the IP (Fig. 1), creating showers responsible for backgrounds along its way. Only a single bunch is simulated to study the directionality which is masked in a case of two colliding beams. When studying the integrated effect, we assume 600 turns as a beam lifetime, that gives for two beams about 10^{15} muons per store passing the IR.

DIRECT $\mu \rightarrow e\nu\tilde{\nu}$ DECAY BACKGROUNDS

Muon decays inside the beam channel create decay electrons and result in a high flux of electromagnetic radiation in the beam pipe. A single bunch will release of order $10^8\ GeV$ per meter of path as muons pass through a detector. Thus the direct decays represent a hardly reducible background in the detectors which has the potential of killing the concept of the muon collider, or at least, redirecting the accelerator work towards parameters involving fewer muons per bunch.

Figure 3 shows calculated e^+e^- energy spectrum in the accelerator components. The huge peak sitting around 1 TeV represents the $\mu \rightarrow e\nu\tilde{\nu}$ decay spectrum with a tail at lower energies enriched by electrons and positrons of electromagnetic showers induced in the beam pipe and superconducting coils. Photons emitted due to synchrotron radiation along e^+e^- tracks in a strong 8 T magnetic field have energy around 1 GeV. The number of photons is about 300 times that for electrons and positrons.

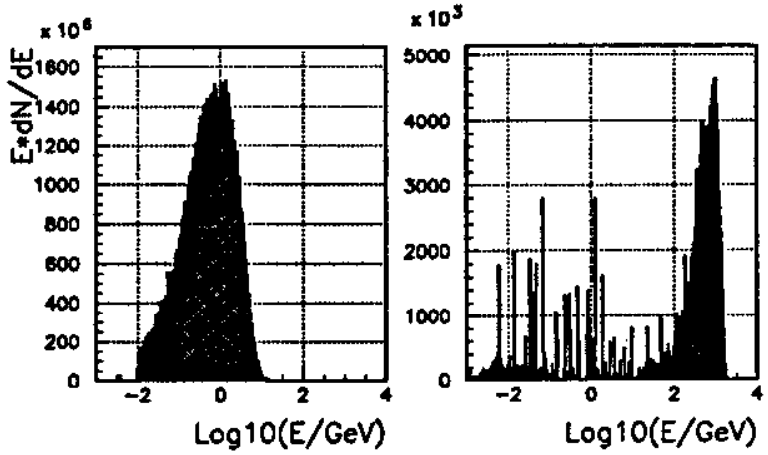

FIGURE 3. Photon (left) and electron/positron (right) energy spectra in the inner triplet accelerator components.

Figure 4 represents energy deposition density in the T1 silicon tracker and first 1.3 meter of the Q3 quadrupole at the either side of the IP. One can see that the energy deposition levels are very high, up to $10^5 - 10^6 GeV/cm^3$ in the innermost parts of the detector. It is clear that one needs to bring these levels down.

To study the source term we have used a tagging techniques in the simulations. Figure 5 shows a distribution of the electromagnetic shower origins: energy deposition in the T1 tracker due to muon decay at distance L from the IP. Due to very high energy of electrons and photons in the large aperture, the whole triplet is a source of backgrounds. There is a strong left(outward)/right(inward) asymmetry in the horizontal plane due to effect of the dipole magnetic field.

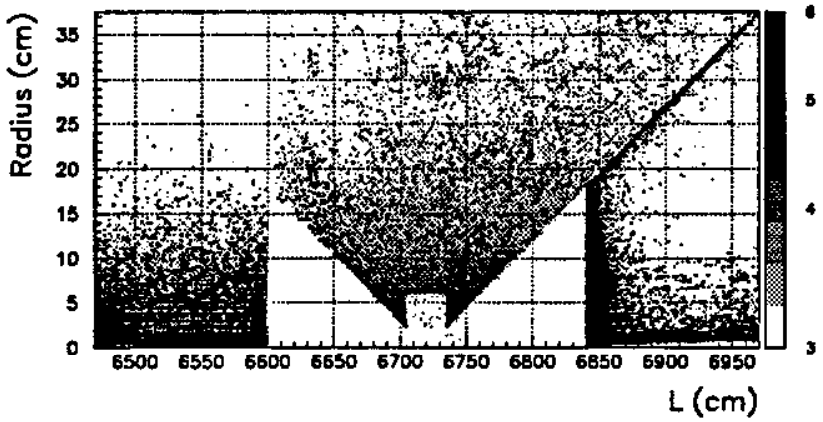

FIGURE 4. Energy deposition in the vicinity of IP, in units of $10^n GeV/cm^3$ per store, where the shade indicates the power n. In this plot muon beam goes from left to right with the IP at L=6720 cm.

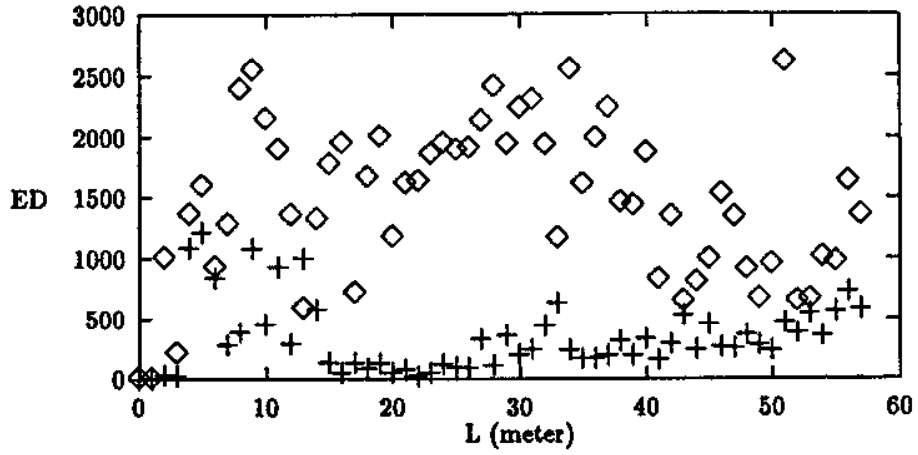

FIGURE 5. Energy deposition (GeV/g per store) in the T1 tracker as a function of distance to the muon decay point. Diamonds are for the outward and pluses are for the inward sides of the tracker.

BACKGROUND REDUCTION WITH COLLIMATORS

The first measure to reduce backgrounds in the detectors was incorporated into the inner triplet lattice from the beginning: a dipole component of the magnetic field in the combined function qudrupoles deflects many of decay electrons into the beam pipe well before the IP. But as it was seen from the previous section, this is not enough. The main job can be done with appropriate collimators.

Several aspects of an effective collimation strategy are clear. The general strategy will involve surrounding all of the the final-focus quads and most of the IR beam pipe with high-Z material. Major variables in this collimator are the inner radius, the distance to which it approaches the interaction point, the angle of the cone which defines the outer surface of the cone (and the angle at which one gives up doing physics). Other variables involve steps and tapers of the inner radius, and covering the collimator with a low-Z cladding.

Since the dominant backgrounds are EM showers with very small transverse momenta, a solenoidal field in the detector will effectively confine all of the charged particles to the vicinity of the beam pipe. Only the low energy, high angle photons at the tails of the EM shower will escape to high radius. Thus the final signal will be an enormous pulse of photons at the critical energy of $\sim 10MeV$.

If the muon decay occurs in the arcs or the superconducting combined-function quad, the decay electron will emit most of its energy as synchrotron photons of energy $\sim 1GeV$ before it hits the beam pipe. If this were the dominant source of background, the most effective collimation strategy might be a "pinhole" collimation very near the IP which limits the solid angle for the synchrotron to emerge from.

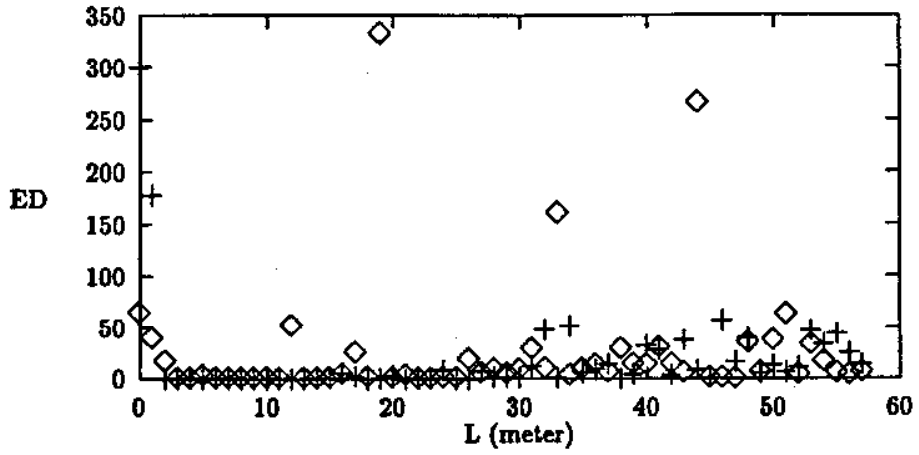

FIGURE 6. Energy deposition (GeV/g per store) in the T1 tracker as a function of distance to the muon decay point with the tungsten nozzle in place. Diamonds are for the outward and pluses are for the inward sides of the tracker.

For muons which decay close to the IP, the decay electron is more likely to survive to initiate a TeV shower when it hits the limiting aperture of the collimator or final focus low-beta quad. For these electrons, additional collimating material is likely to act as an amplifier which causes TeV showers to emerge from the quads right at at shower-maximum. If this were the dominant source of background, the most effective collimation would include a limiting aperture of order 1m from the IP, with an interior conical surface which opens outward as it approaches the IP. These collimators would then have the aspect of two nozzles spraying electromagnetic fire at each other, with the charged component of the EM showers being confined radially by the solenoidal magnetic field and the photons from one nozzle being trapped (to whatever degree possible) by the conical opening in the opposing nozzle.

In this paper we studied collimators of a few configurations occupied the cone $\theta < 150mrad$ in the $15 < L < 120cm$ region on the either side of the IP (Fig. 2). Collimators made of tungsten as well as of a combination of various materials (aluminum, copper and tungsten) with different shapes of the hole have been considered. It turns out that for the main source of the backgrounds, direct muon decays, the best choice is a tungsten nozzle with an aperture radius R=0.45 cm at L=120 cm and R=1 cm at L=15 cm. Figure 6 shows how significant background reduction is in this case. There is a significant difference in the background levels in the left (outward) and in the right (inward) parts of the tracker and calorimeter. This depends on the magnetic field, nozzle and collimator configurations. Calculated absorbed doses in six regions of the detector are given in Table 1.

Muon decays along the whole triplet do contribute into the backgrounds in the detector (Fig. 5 and 6). So, an additional way to suppress further the background levels can be a collimator between Q3 and B3 with a smallest possible aperture. A

Table 1: Dose (mrad/store) absorbed in the left(L) and right(R) parts of the detector for the cases with and without tungsten nozzle and with and without copper collimator.

Nozzle	Collimator	T1 (L)	T1 (R)	T2 (L)	T2 (R)	CH (L)	CH (R)
No	No	1360	326	25	9.89	0.534	0.238
No	Yes	267	108	5.5	3.81	0.075	0.079
Yes	No	22.2	17.6	0.656	0.480	0.074	0.036
Yes	Yes	2.77	7.68	0.050	0.037	0.032	0.006
	K_{max} =	491	43	498	269	17	38

copper collimator 50 cm long with 2.5σ radius aperture in these calculations provided up to a factor of 10 additional dose reduction (see Table 1). The total maximum reduction K_{max} defined as a ratio of background levels in the given detector region without protective measures to that with a tungsten nozzle and copper collimator between Q3 and B3 magnets is given in the last row of the Table 1. It is as high as a factor of 500 on the best, but for the larger radii in calorimeter it is "only" a factor of 20 to 40. Particle spectra in detector are very soft in such a configuration: for all the considered regions background photons and electrons have energy below 100 MeV, being on the average just a few MeV (Fig. 7).

The e^+e^- fluence is given in Table 2 for the crossing of two 10^{12} muon beams. It turns out that the charged particle fluxes calculated as the total track length in the region divided by the region volume, and as the averaged energy deposition density in the region divided by the minimum ionizing power of the region material, coincide within 20-30 percent for small radii and within a few percent for large radii. The behavior in different detector regions is similar to the dose. Maximum reduction is again of about a factor of 500. With an optimal collimation the peak charged

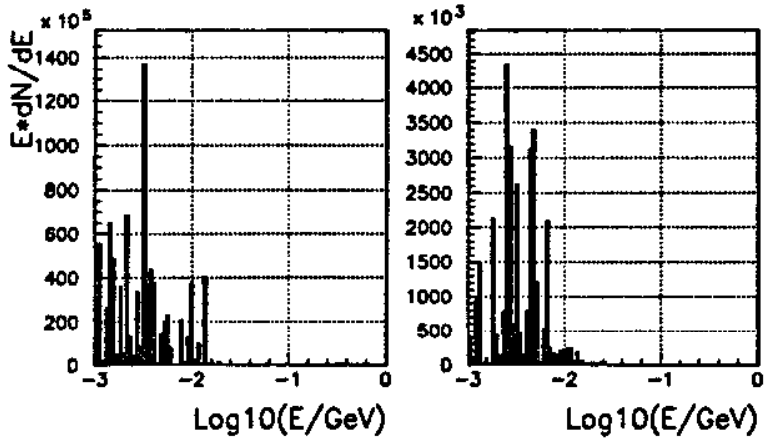

FIGURE 7. Photon (left) and electron/positron (right) energy spectra in the CH calorimeter region with the tungsten nozzle in place.

Table 2: The e^+e^- fluence (cm^{-2} per crossing) in the left(L) and right(R) parts of the detector for the cases with and without tungsten nozzle and with and without copper collimator. Fluence is defined here as a calculated energy deposition density over $(dE/dx)_{min}$ for Si and CH, respectively.

Nozzle	Coll	T1 (L)	T1 (R)	T2 (L)	T2 (R)	CH (L)
No	No	8.54×10^4	2.04×10^4	1.57×10^3	6.21×10^2	2.86×10^1
No	Yes	1.68×10^4	6.74×10^3	3.46×10^2	2.38×10^2	4.00×10^0
Yes	No	1.40×10^3	1.10×10^3	4.11×10^1	3.02×10^1	3.93×10^0
Yes	Yes	1.74×10^2	4.81×10^2	3.15×10^0	2.31×10^0	1.73×10^0

particle flux in the silicon tracker is of the order of 500 cm^{-2} per crossing of two single bunches through the IR in opposite directions. The fluxes fall down very rapidly with radius.

BEAM HALO BACKGROUNDS

These arise from muons which are lost some distance upstream of the detectors. A noninteracting muon which passes through the detector will be of little consequence. However, muons which induce electromagnetic or hadronic showers either upstream or inside of the detector will cause more serious problems. Beam particles injected with large momentum errors or betatron amplitudes will be lost within the first few turns. After this, an equilibrium level of losses will be attained as particles are promoted to larger betatron amplitudes via beam disruption from the collision point, a beam-gas scattering, etc.

In principle the halo background can be calculated fairly accurately in the muon collider. This is due to the small number of turns ($\sim$ 1000) which must be tracked before the muons decay. In contrast, the halo losses in hadron colliders develop over many millions of turns and depend on things like RF noise, magnet power supply ripple moving particles repeatedly over high-order resonances, and other imponderables. These effects do not have time to become significant in the muon collider, and the small number of turns can be tracked numerically to adequate accuracy. However, this simulation will require a detailed knowledge of the machine lattice and a reasonable optimization of the scraping strategy. This will be one of the major projects in the coming months.

At this stage we simulated the beam as entering the IR with a non-truncated Gaussian profile. Muons outside $\pm 3\sigma$ will then interact and be scraped by the final arc magnets, low-beta quads, collimators, and detector components. Figure 8 shows a distribution of the muon interaction vertices in the vertical plane in the vicinity of the IP. The distribution is pretty symmetric, but in the horizontal plane there is a strong asymmetry related to the magnetic field. With an energy cut-off for this plot equal to 100 MeV, more than 90% of the vertices are direct e^+e^- pair production,

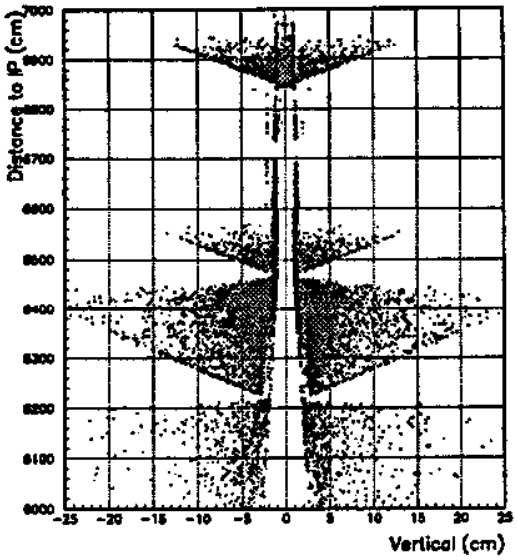

FIGURE 8. Muon beam halo interaction points in the components in the vicinity of the IP with the tungsten nozzle in place. The distribution is given for the vertical plane. In this plot the IP corresponds to L=6720 cm. The muon beam goes from bottom to top.

about 5% are muon bremsstrahlung, and less than a few percent are for deep inelastic nuclear interactions, muon decays and energetic knock-on electron production. For the considered Q3 quadrupole configuration with its aperture decreasing toward the IP (creating the bottleneck for out-of-axis particles), all the contribution to the background in a detector from the beam halo comes from less then about 5 meters upstream of the IP, very different of the direct decay source. So, a copper collimator between Q3 and B3 is useless for this source. Background reduction with a tungsten nozzle is only about a factor of 4. The left(outward)/right(inward) asymmetry is even stronger, with right regions always in a worse condition. With a considered $\pm 3\sigma$ beam loss model background levels are 10 to 100 times higher compared to the best protected configuration in the case of direct decays. So, obviously more work is needed toward a dedicated beam scraper system well upstream of the IR.

EFFECT OF BACKGROUNDS ON DETECTOR PERFORMANCE

The two detector capabilities most at risk from the unavoidable "direct" $\mu \rightarrow e\nu\tilde{\nu}$ decay induced background are the tracking capability (particularly at low radius) and the calorimetry energy measurement. In both cases the background arises from the enormous pulse of $\sim 10 MeV$ photons, essentially all which emerge from the unshielded gap between the collimator cones at the interaction point. As hoped, the

Table 3: Averaged occupancy (percent per crossing) T1 and T2 silicon pixels for the direct muon decays of two 10^{12} beams in the left (L) and right(R) parts of the detector for the cases with and without tungsten nozzle and with and without copper collimator.

Nozzle	Collimator	T1 (L)	T1 (R)	T2 (L)	T2 (R)
No	No	34.16	8.16	23.55	9.32
No	Yes	6.72	2.70	5.19	3.57
Yes	No	0.56	0.44	0.62	0.45
Yes	Yes	0.07	0.19	0.05	0.03

combination of the shielding, collimators, and the solenoidal field seems to completely eliminate higher energy gammas and most of charged particles of all momenta.

Silicon Tracker

The inner tracker must be a pixellated silicon detector for reasons that will be evident below. The background in this device will then have the random "salt and pepper" flavor of uncorrelated hits from low energy photons which convert in one plane of silicon, then spiral around with a gyroradius of a few centimeters before coming to rest. With a sufficient tracking redundancy and a low enough density of hits, there should be no mistaking these for high-momentum tracks from physics events. Survival of the tracking measurement relies on preserving a low enough "occupancy" (fraction of hit pixels) to guarantee a high efficiency for the "good" hits from the high momentum tracks from beam-beam interactions. The reconstruction efficiency of a typical tracking device will not suffer as long as the occupancy is less than 1%. Tracking efficiencies typically begin to suffer at occupancies somewhere between 1% and 20% depending on the redundancy and resolution of the tracking system.

Table 3 shows the averaged occupancy calculated from the direct decay source for a silicon tracker with $20\mu m \times 20\mu m$ pixels in the inner tracker (T1) and with $50\mu m \times 300\mu m$ pixels in the outer tracker T2. One can see that the tracking occupancy (fraction of hits per pixel per crossing) is of order 0.1% to 0.2% for the optimized collimation scheme. This should be adequate to ensure the survival and correct function of the inner tracker — a significant conclusion.

Some comments are appropriate about the pixel sizes assumed, which are of course critical to calculating the occupancy. The $20\mu m \times 20\mu m$ dimensions are consistent with current technology for serial readout "CCD" style silicon detectors. The "smart pixels" under development for hadron colliders will be at least an order of magnitude larger. However, for the muon collider there is no need for the "dead-timeless" readout of the smart pixels given the $\sim 20\mu sec$ time between crossings and the small rate of physics events. Thus these pixel sizes, although adequate to

the task, represent rather conservative assumptions about what should be possible by the start of the next millennium.

With the best collimation described above, the radiation dose in the innermost layers of pixels is approximately 0.1-0.5 Mrad/yr compared to almost 10 Mrad/yr at the LHC [7], so that electronics survival is not a likely problem.

Calorimeter

The calorimeter energy deposition is approximately 10^6 GeV per beam crossing even for the best-case shielding and collimation we have developed. This is daunting to say the least. However, consider the following argument, which is intended to make it plausible that one could learn to live with this. All of the 1000 TeV of energy appears as 10 MeV photons, so that to first order this appears as more-or-less uniform of "pedestal offset" in the first depth segment of each tower of the electromagnetic (EM) calorimeter. If necessary, the size of this pedestal can be determined on an even-by-event basis and subtracted out from the observed energy in any tower which is suspected of having a physics signal; towers below some threshold corresponding to a few sigma energy fluctuation will be ignored. Now, pedestal sigma from the flood of gammas grows as the square root of the tower area, whereas the signal from a well-localized electron or photon shower is independent of tower size. Thus one wins in signal/noise by reducing the EM tower size until the tower size is reduced to dimensions comparable to the Moliere radius (the transverse width of the EM shower in the calorimeter). These considerations push towards placing the calorimeter at the highest affordable radius. A reasonable system might contain approximately 10^5 electromagnetic towers a few centimeters in size for a calorimeter at a radius of 2 meters. Each of these 10^5 towers will then receive 10 GeV of energy each crossing, in the form of approximately one thousand 10-MeV gammas. Assuming Gaussian statistics on the number of incident photons, the fluctuation in this energy will be approximately $10GeV/\sqrt{(1000)} = 300MeV$. This is less than the pedestal noise in "fast" liquid argon.

Those who might feel that the last argument was a little to glib might be interested in speculations on ways to discriminate further against the background in the calorimeter. A first readily apparent handle is the depth profile in the EM calorimeter: the 10 MeV gammas interact mainly at the front of the EM tower whereas shower maximum for a 100-GeV electron is much deeper. Appropriate weighting and fitting of the shower profile might provide a factor of 3 to 5 more rejection than a simple pedestal subtraction. A second less readily apparent handle is the directionality of the background gammas, which emanate not from the IP but from the tips of the collimators a few centimeters away. If sufficiently directional calorimetry could be obtained (similar to collimators on a gamma-ray telescope) for the first few radiation lengths of the EM calorimeter, then a valuable additional factor might be obtained.

Electron machines have learned to coexist with the flood of keV gammas from synchrotron radiation which accompany each beam crossover, and in the end it does not appreciably interfere with their ability to do physics in the GeV range. Perhaps it is best to view the flood of MeV gammas accompanying the beam crossovers in muon colliders as the "synchrotron radiation" of TeV physics.

CONCLUSIONS

- We have completed a first-pass investigation of the backgrounds from "direct" $\mu \rightarrow e\nu\tilde{\nu}$ decays in a simplified detector geometry. The most effective shielding and collimation geometry that we have devised eliminated all but the low-energy gammas from the tails of electromagnetic showers, and reduced this background by a factor of 50 to 500 compared to the unshielded case.
- This background gives rise to about 500 tracks per cm^{-2} per crossing. This is painful but not fatal to a pixel detector at the innermost radius of the tracker.
- Energy deposited in the calorimeter is about 1000 TeV per crossing, all of it in the first depth segment(s) of the EM calorimeter. Strategies for dealing with this involve segmenting the EM calorimeter as finely as possible and putting it at a large radius.
- We have begun to characterize the beam halo induced backgrounds, but much work remains to be done. Further work on the collider lattice and on a beam scraper system is needed.
- Detector model sophistication and study of photo-hadron and photo-muon contributions to the background levels are in progress.

ACKNOWLEDGMENTS

We thank Robert Palmer and John Peoples for inducing our interest in this problem, Sergei Striganov for his crucial contribution to the muon interaction algorithms, Pat Colestock and David Finley for their support of this work.

References

[1] Cline, D., *Nucl. Instruments and Methods* **A350**, 24-26 (1994).

[2] Neuffer, D., and Palmer, R., "A High-Energy High-Luminosity $\mu^+\mu^-$ Collider", *Preprint BNL-61267*, 1994.

[3] Mokhov, N., "Accelerator-Experiment Interface at Hadron Colliders: Energy Deposition in the IR Components and Machine Related Background to Detectors", *FERMILAB-Pub-94/085*, 1994.

[4] Mokhov, N., "The MARS95 Code System", *Fermilab FN*, 1995.

[5] Mokhov, N., "The MARS10 Code System: Inclusive Simulation of Hadronic and Electromagnetic Cascades and Muon Transport", *Fermilab FN-509*, 1989; Mokhov, N., "The MARS12 Code System", in *Proceedings of the SARE Workshop*, Santa Fe, January 1993.

[6] Striganov, S., *Nucl. Instruments and Methods* **A322**, 225-230 (1992); "Fast Precise Algorithm for Simulation of Ionization Energy Losses", *IHEP 92-80*, Protvino, 1992.

[7] "The Compact Muon Solenoid", *CERN/LHCC 94-38*, 1994.